Proceedings World Geothermal Congress 2020+1
Reykjavik, Iceland, April – October, 2021

Uncertainty Quantification of Highly-Parameterized Geothermal Reservoir Models Using Ensemble-Based Methods

Elvar K. Bjarkason[1,2], Oliver J. Maclaren[2], Ruanui Nicholson[2], Angus Yeh[2] and Michael J. O'Sullivan[2]

[1]Institute of Fluid Science, Tohoku University, Sendai, Miyagi 980-8577, Japan

[2]Department of Engineering Science, The University of Auckland, Auckland 1010, New Zealand

e.bjarkason@tohoku.ac.jp

Keywords: Uncertainty quantification, geothermal modelling, randomized maximum likelihood, ensemble smoothers, randomized matrix algorithms, adjoint methods.

ABSTRACT

Geothermal reservoir simulations are typically time-consuming, and models made up of a few tens of thousands of model blocks can easily take hours to run. This is a considerable hindrance to model development and uncertainty quantification since current industry standard methods require running numerous simulations to invert or history-match a highly-parameterized geothermal model. Extensive uncertainty quantification using standard Markov chain Monte Carlo sampling is generally not viable in the case of a highly-parameterized geothermal model since it usually requires a significant number of simulations. Because of computational limitations in terms of time and resources, parameter uncertainty in subsurface transport models is often quantified using a limited number or a small ensemble of different numerical models. Here we explore using ensemble-based methods for approximating model parameter and predictive uncertainty in the context of models describing high-enthalpy geothermal reservoirs. First, we consider using a randomized maximum likelihood approach where we apply a recently developed randomized Levenberg-Marquardt (LM) approach to efficiently invert an ensemble of models. The randomized LM method combines adjoint code and randomized low-rank matrix factorization methods to facilitate rapid inversion of highly-parameterized models. Second, we contrast this approach with iterative ensemble smoothers, which do not require adjoint code. Both methods are well suited to high-performance parallel computing environments. Finally, we compare these two approaches with using simple local sensitivity analysis.

1. INTRODUCTION

This study considers the applicability of ensemble-based methods for uncertainty quantification of models describing high-enthalpy, convective geothermal reservoirs. When applying an ensemble-based approach, to estimate model uncertainty, the target is to generate a set or ensemble of different models (say 100 models) which adequately describe or match observations of the system represented by those models. The model uncertainty is then approximately characterized by the variability of the resulting ensemble of models.

Ensemble-based methods have been used to describe model uncertainty in various large-scale modelling contexts, such as weather prediction (Houtekamer & Mitchell, 2005; Miyoshi et al., 2016), petroleum reservoir modelling (Chen & Oliver, 2014) and groundwater modelling (White, 2018). Experience with using ensemble methods for uncertainty quantification of geothermal reservoir models is limited, however. Onur & Tureyen (2006), Tureyen & Onur (2010), and Tureyen et al. (2014) applied the randomized maximum likelihood (RML) method (Oliver et al., 1996) to generate an ensemble of lumped-parameter reservoir models for uncertainty quantification of water-level changes in low-temperature geothermal systems. RML has also been applied to synthetic geothermal production simulations where the simulations are initialized with fixed initial conditions (Omagbon, 2018; Zhang et al., 2014). Tureyen & Onur (2011) applied another ensemble-based method called the ensemble Kalman filter (EnKF) (Evensen, 1994, 2009) to uncertainty quantification of lumped-parameter models describing the Balcova-Narlidere geothermal field in Turkey. Vogt et al. (2012) used the EnKF to assimilate data from a tracer experiment carried out at the enhanced geothermal system at Soultz-sous-Forêts, France. Using the EnKF, they generated an ensemble of models having different permeability distributions and used these models for uncertainty quantification of future production temperatures. All these geothermal studies considered processes described solely by transient production simulations.

Here we look at applying ensemble-based methods to combined natural-state and production models, commonly used to model high-enthalpy, convective geothermal systems. Those models involve solving a nonlinear steady-state simulation problem to describe the natural-state of a geothermal system which exists prior to production commencing. The simulated natural-state conditions are then used as initial conditions for the production simulation. For this type of problem, we look at applying RML and iterative ensemble smoothers to generate an ensemble of plausible models which are consistent with measured data. We do not consider the EnKF as it is designed for sequential in time data assimilation of transient models.

The following section describes the uncertainty quantification methods considered here, which include RML, two iterative ensemble smoothers and the Laplace approximation (local sensitivity analysis). To generate an ensemble of N_e models conditioned to observations, the RML method requires solving a separate inversion or calibration problem for each ensemble member. We solve each inverse problem using a recently developed randomized Levenberg-Marquardt inversion algorithm (Bjarkason et al., 2018; Bjarkason, 2019) which combines adjoint and direct code (Bjarkason et al., 2019, 2014, 2015, 2016) with randomized matrix algorithms (Bjarkason, 2019; Halko et al., 2011) to enable efficient inversion of highly-parameterized reservoir models. We run the ensemble of RML inversions independently in parallel on a computing cluster.

The iterative ensemble smoothers, on the other hand, do not use direct or adjoint code. Instead, iterative ensemble smoothers simultaneously update the model parameters of all the ensemble members based on the relationship between the model parameters

and simulated model outputs of the ensemble. This gives iterative ensemble smoothers an advantage over using the RML approach used here (which uses adjoint code) since ensemble smoothers can in principle be model-independent and treat the forward simulator as a black box. The main computational expense of updating an ensemble of models using an ensemble smoother involves running N_e reservoir simulations. The first iterative ensemble smoother we use is an implementation of the Levenberg-Marquardt (LM) form of the ensemble RML (EnRML) method (Chen & Oliver, 2013). The implementation we use is called PEST++IES (pestpp-ies) (White, 2018) and is freely available as part of the PEST++ software suite (Welter et al., 2015). An advantage of PEST++IES is that it uses PEST (Doherty, 2015, 2016) file format. Transitioning to using PEST++IES should, therefore, be relatively straightforward for geothermal modellers that are familiar with using standard PEST. The second iterative ensemble smoother we try out is the ensemble smoother with multiple data assimilation (ESMDA) (Emerick & Reynolds, 2013). We apply our ESMDA implementation based on recommendations given in (Emerick, 2016, 2019). We are not aware of any previous studies that have applied iterative ensemble smoothers to geothermal reservoir modelling. We, therefore, consider this as a preliminary study to establish how applicable iterative ensemble smoothers are in the geothermal context at hand.

We compare the RML approach with the iterative ensemble smoothers by applying them to a synthetic geothermal reservoir model based on the one used in (Bjarkason et al., 2018, 2016). Additionally, we compare the ensemble-based uncertainty quantification methods with using the Laplace approximation (also known as local linear analysis), which is the method most commonly used for uncertainty quantification of geothermal models. We look at how well the models generated by the methods match historical observations and we consider how reliably the methods can predict future values of production enthalpies.

2. UNCERTAINTY QUANTIFICATION METHODS

2.1 Preliminaries

Observation noise and prior ideas about model parameters are commonly described using Gaussian statistics. Therefore, we will assume Gaussian statistics for both observation noise and model priors. In the following sections, we use $\boldsymbol{x}\sim\mathcal{N}(\bar{\boldsymbol{x}},\boldsymbol{C}_{\mathrm{x}})$ to denote a vector $\boldsymbol{x}$ which is randomly drawn from a Gaussian distribution with mean $\bar{\boldsymbol{x}}$ and covariance $\boldsymbol{C}_{\mathrm{x}}$.

2.2 Laplace Approximation

The so-called Laplace approximation or local linear analysis is the most commonly used method when estimating parameter uncertainty in a geothermal reservoir model (see, e.g., Doherty et al. (2017) and Omagbon (2018)). In practice, it typically involves applying local sensitivity analysis at the current "best" parameter estimate. The "best" parameter estimate will in practice be the set of model parameters which out of all the tested combinations of parameters give the most suitable match to observations. Then the local sensitivity analysis is used to describe model uncertainty. Omagbon (2018) advocated using the Laplace approach since it only requires inverting a single model to find a "best" parameter estimate. Model uncertainty may, therefore, be quantified at a relatively low cost. However, as we discuss later, the cost of using an iterative ensemble smoother for uncertainty quantification may not necessarily be greater than the cost of inverting a single model using inversion tools commonly used in practice (such as PEST (Doherty, 2015, 2016) or iTOUGH2 (Finsterle, 2007; Finsterle & Pruess, 1995)).

To be more precise, for generating approximate posterior samples using the Laplace approach, we first find a maximum a posteriori parameter (MAP) estimate $\boldsymbol{m}_{\mathrm{MAP}}$ and then sample around it. The MAP ($\boldsymbol{m}_{\mathrm{MAP}}$) is defined as the set of parameters that minimize the following objective function

$$\Phi(\boldsymbol{m}) = \Phi_{\mathrm{d}}(\boldsymbol{m}) + \Phi_{\mathrm{m}}(\boldsymbol{m}) \tag{1}$$

where

$$\Phi_{\mathrm{d}}(\boldsymbol{m}) = [\boldsymbol{d}(\boldsymbol{m}) - \boldsymbol{d}_{\mathrm{obs}}]^T \boldsymbol{C}_{\mathrm{d}}^{-1} [\boldsymbol{d}(\boldsymbol{m}) - \boldsymbol{d}_{\mathrm{obs}}] \quad \text{and} \quad \Phi_{\mathrm{m}}(\boldsymbol{m}) = \left[\boldsymbol{m} - \boldsymbol{m}_{\mathrm{pr}}\right]^T \boldsymbol{C}_{\mathrm{m}}^{-1} \left[\boldsymbol{m} - \boldsymbol{m}_{\mathrm{pr}}\right] \tag{2}$$

Here $\boldsymbol{d}_{\mathrm{obs}}$ is the vector of N_d observations, $\boldsymbol{d}(\boldsymbol{m})$ denotes the simulated observations using the vector of N_m model parameters $\boldsymbol{m}$, $\boldsymbol{C}_{\mathrm{d}}$ is the observation covariance matrix, $\boldsymbol{m}_{\mathrm{pr}}$ denotes the prior parameter mean, and $\boldsymbol{C}_{\mathrm{m}}$ is the prior parameter covariance matrix.

For minimizing (1), we use a randomized LM method (Bjarkason et al., 2018; Bjarkason, 2019). We base model updates on transformed model parameters given by $\tilde{\boldsymbol{m}} = \boldsymbol{L}^{-1}\left(\boldsymbol{m} - \boldsymbol{m}_{\mathrm{pr}}\right)$, where $\boldsymbol{L}$ is the Cholesky matrix which satisfies $\boldsymbol{C}_{\mathrm{m}} = \boldsymbol{L}\boldsymbol{L}^T$. Defining the dimensionless sensitivity matrix $\boldsymbol{S}_{\mathrm{D}} = \boldsymbol{C}_{\mathrm{d}}^{-1/2}\boldsymbol{S}\boldsymbol{L}$ (where $\boldsymbol{S} = \partial\boldsymbol{d}(\boldsymbol{m})/\partial\boldsymbol{m}$ is the standard N_d by N_m sensitivity matrix) we update the model parameters at the kth iteration according to

$$\tilde{\boldsymbol{m}}^{k+1} = \tilde{\boldsymbol{m}}^k - \left[\boldsymbol{S}_{\mathrm{D}}^T\boldsymbol{S}_{\mathrm{D}} + (1+\gamma)\boldsymbol{I}_{N_m}\right]^{-1}\left(\boldsymbol{S}_{\mathrm{D}}^T\boldsymbol{C}_{\mathrm{d}}^{-1/2}[\boldsymbol{d}(\tilde{\boldsymbol{m}}^k) - \boldsymbol{d}_{\mathrm{obs}}] + \tilde{\boldsymbol{m}}^k\right) \tag{3}$$

We solve the above model update equation approximately by finding a low-rank approximation of $\boldsymbol{S}_{\mathrm{D}}$ using randomized singular-value decomposition (Bjarkason, 2019; Halko et al., 2011). We form the low-rank approximation using a randomized 2-view method (Bjarkason et al., 2018; Bjarkason, 2019; Halko et al., 2011), which costs $r+l$ adjoint solves and $r+l$ direct solves. Here r is the rank of the approximation and l is an oversampling factor to improve the accuracy of the randomized algorithm. When both N_d and N_m are large, and $r+l \ll N_d, N_m$, we can form the low-rank approximation of $\boldsymbol{S}_{\mathrm{D}}$ at a much lower cost than forming the full sensitivity matrix $\boldsymbol{S}$, which would cost at least N_d adjoint solves or N_m direct solves. The cost of forming $\boldsymbol{S}$ would be even higher when forming $\boldsymbol{S}$ by finite differencing as it would cost at least N_m nonlinear reservoir simulations.

After finding the MAP estimate, the Laplace approach approximates posterior parameter uncertainty or variability by a posterior covariance matrix given by

$$\boldsymbol{C}_{\text{post}} = \left[\boldsymbol{S}^T\boldsymbol{C}_{\text{d}}^{-1}\boldsymbol{S} + \boldsymbol{C}_{\text{m}}^{-1}\right]^{-1} = \boldsymbol{L}\left[\boldsymbol{S}_{\text{D}}^T\boldsymbol{S}_{\text{D}} + \boldsymbol{I}_{N_m}\right]^{-1}\boldsymbol{L}^T \tag{4}$$

Accordingly, Laplace posterior samples are given by $\boldsymbol{m}_j \sim \mathcal{N}(\boldsymbol{m}_{\text{MAP}}, \boldsymbol{C}_{\text{post}})$. To generate the samples we evaluate $\boldsymbol{m}_j = \boldsymbol{m}_{\text{MAP}} + \boldsymbol{C}_{\text{post}}^{1/2}\boldsymbol{z}_{\text{rand},j}$, where $\boldsymbol{z}_{\text{rand},j} \sim \mathcal{N}(\boldsymbol{0}, \boldsymbol{I}_{N_m})$. We can form $\boldsymbol{C}_{\text{post}}^{1/2}$, for instance, via a Cholesky- or eigen-decomposition of $\boldsymbol{C}_{\text{post}}$. Alternatively, we can find an approximate truncated singular-value decomposition (TSVD) of $\boldsymbol{S}_{\text{D}} \approx \boldsymbol{U}_r\boldsymbol{\Lambda}_r\boldsymbol{V}_r^T$ (e.g., using the generalized randomized subspace iteration method in (Bjarkason, 2019)), where $\boldsymbol{\Lambda}_r$ is an r by r diagonal matrix containing estimates of the principal singular values of $\boldsymbol{S}_{\text{D}}$, and $\boldsymbol{U}_r$ and $\boldsymbol{V}_r$ contain estimates of the principal left- and right-singular vectors of $\boldsymbol{S}_{\text{D}}$, respectively. Then we can find approximate posterior samples using (Petra et al., 2014)

$$\boldsymbol{m}_j = \boldsymbol{m}_{\text{MAP}} + \boldsymbol{C}_{\text{post}}^{1/2}\boldsymbol{z}_{\text{rand},j} \approx \boldsymbol{m}_{\text{MAP}} + \boldsymbol{L}\left\{\boldsymbol{V}_r\left[(\boldsymbol{\Lambda}_r + \boldsymbol{I}_r)^{-1/2} - \boldsymbol{I}_r\right]\boldsymbol{V}_r^T + \boldsymbol{I}_{N_m}\right\}\boldsymbol{z}_{\text{rand},j} \tag{5}$$

A drawback of using the Laplace approximation for generating posterior parameter samples is that the samples often result in bad matches to observations (Liu & Oliver, 2003). This was also the case for the experiments presented here. A model that results in bad matches to observations suggests that it has parameters that are unlikely to be a good representation of the truth. Therefore, it may potentially be a bad idea to base model predictions on an ensemble of models generated by the Laplace approximation. However, for the results presented here, using the Laplace approximation resulted in prediction intervals that encapsulated the true production enthalpies well.

2.3 Randomized Maximum Likelihood

Applying RML, we solve a stochastically generated minimization problem for each ensemble member. That is for $j = 1, \cdots, N_e$ we draw random observations $\boldsymbol{d}_{\text{obs},j} \sim \mathcal{N}(\boldsymbol{d}_{\text{obs}}, \boldsymbol{C}_{\text{d}})$ and a random prior sample $\boldsymbol{m}_{\text{uc},j} \sim \mathcal{N}(\boldsymbol{m}_{\text{pr}}, \boldsymbol{C}_{\text{m}})$. The jth RML sample is generated by finding the minimum of

$$\Phi_j(\boldsymbol{m}_j) = \Phi_{\text{d}}^j(\boldsymbol{m}_j) + \Phi_{\text{m}}^j(\boldsymbol{m}_j) \tag{6}$$

where

$$\Phi_{\text{d}}^j(\boldsymbol{m}_j) = \left[\boldsymbol{d}(\boldsymbol{m}_j) - \boldsymbol{d}_{\text{obs},j}\right]^T\boldsymbol{C}_{\text{d}}^{-1}\left[\boldsymbol{d}(\boldsymbol{m}_j) - \boldsymbol{d}_{\text{obs},j}\right] \quad \text{and} \quad \Phi_{\text{m}}^j(\boldsymbol{m}_j) = \left[\boldsymbol{m}_j - \boldsymbol{m}_{\text{uc},j}\right]^T\boldsymbol{C}_{\text{m}}^{-1}\left[\boldsymbol{m}_j - \boldsymbol{m}_{\text{uc},j}\right] \tag{7}$$

Like finding a MAP estimate, we also use the randomized LM approach mentioned above to minimize (6). When applying the updating formula (3) to update the jth ensemble member, we only need to replace $\boldsymbol{m}_{\text{pr}}$ with $\boldsymbol{m}_{\text{uc},j}$ and $\boldsymbol{d}_{\text{obs}}$ with $\boldsymbol{d}_{\text{obs},j}$.

Each RML inversion using a gradient-based method such as LM is not guaranteed to converge to a solution that minimizes the objective function in (6). Furthermore, a lack of convergence will generally be the case in practice where the number of model updates and allocated time will be limited. Therefore, it is common to discard ensemble members that result in insufficient matches to observations. A criterion commonly used is to discard ensemble members that do not satisfy (Oliver et al., 2008)

$$\Phi_{\text{N}}(\boldsymbol{m}_j) \leq 1 + 5\sqrt{2/N_d} \tag{8}$$

where $\Phi_{\text{N}}(\boldsymbol{m}_j) = \Phi_{\text{d}}(\boldsymbol{m}_j)/N_d$ denotes the normalized observation mismatch. When presenting posterior prediction results for the RML method we discard all ensemble members that do not satisfy (8).

2.4 Iterative Ensemble Smoothers

2.4.1 EnRML

Iterative ensemble smoothers aim to find an ensemble of N_e models, where the jth model realization approximately minimizes (6). As in the case of RML we draw random observation and prior realizations according to $\boldsymbol{d}_{\text{obs},j} \sim \mathcal{N}(\boldsymbol{d}_{\text{obs}}, \boldsymbol{C}_{\text{d}})$ and $\boldsymbol{m}_{\text{uc},j} \sim \mathcal{N}(\boldsymbol{m}_{\text{pr}}, \boldsymbol{C}_{\text{m}})$. Define the ensemble matrices $\boldsymbol{D}_k = \left[\boldsymbol{d}(\boldsymbol{m}_1^k), \cdots, \boldsymbol{d}(\boldsymbol{m}_{N_e}^k)\right]$, $\boldsymbol{M}_k = \left[\boldsymbol{m}_1^k, \cdots, \boldsymbol{m}_{N_e}^k\right]$, $\boldsymbol{M}_0 = \boldsymbol{M}_{\text{pr}} = \left[\boldsymbol{m}_{\text{uc},1}, \cdots, \boldsymbol{m}_{\text{uc},N_e}\right]$, and

$$\Delta\boldsymbol{M}_{\text{pr}} = \frac{1}{\sqrt{N_e - 1}}\left(\boldsymbol{M}_{\text{pr}} - \bar{\boldsymbol{M}}_{\text{pr}}\right);\ \Delta\boldsymbol{M}_k = \frac{1}{\sqrt{N_e - 1}}\left(\boldsymbol{M}_k - \bar{\boldsymbol{M}}_k\right);\ \Delta\boldsymbol{D}_k = \frac{1}{\sqrt{N_e - 1}}\left(\boldsymbol{D}_k - \bar{\boldsymbol{D}}_k\right) \tag{9}$$

With the above definitions, then model updates of the Gauss-Newton or LM forms of iterative ensemble smoothers can be written in terms of an ensemble representation of a sensitivity matrix given by

$$\boldsymbol{S}_{e,k} = \Delta\boldsymbol{D}_k(\Delta\boldsymbol{M}_k)^{\dagger} \tag{10}$$

where $\boldsymbol{X}^{\dagger}$ denotes the pseudoinverse of $\boldsymbol{X}$.

Model updates using the Gauss-Newton form of the iterative ensemble smoother called EnRML (Chen & Oliver, 2013) can be written as

$$\boldsymbol{m}_j^{k+1} = \boldsymbol{m}_j^k + \beta_k\left\{\boldsymbol{m}_j^{\text{pr}} - \boldsymbol{m}_j^k + \Delta\boldsymbol{M}_{\text{pr}}\Delta\boldsymbol{M}_{\text{pr}}^T\boldsymbol{S}_{e,k}^T\left[\boldsymbol{S}_{e,k}\Delta\boldsymbol{M}_{\text{pr}}\Delta\boldsymbol{M}_{\text{pr}}^T\boldsymbol{S}_{e,k}^T + \boldsymbol{C}_{\text{d}}\right]^{-1}\left(\boldsymbol{d}_{\text{obs},j} - \boldsymbol{d}(\boldsymbol{m}_j^k) - \boldsymbol{S}_{e,k}\left(\boldsymbol{m}_j^{\text{pr}} - \boldsymbol{m}_j^k\right)\right)\right\} \tag{11}$$

where β_k is a line-search or step-length parameter. As mentioned before, we apply an LM implementation of EnRML called PEST++IES (White, 2018), which is an implementation of the LM-EnRML algorithm proposed by (Chen & Oliver, 2013).

In the above, we have given a brief outline of an iterative ensemble smoother. Practical implementations usually involve finding model updates based on the TSVD of various matrices and some form of localization to regulate model updates (see. e.g., (Chen & Oliver, 2013, 2014, 2016)). Localization is usually considered necessary to increase the degrees of freedom to match observations adequately and to improve the variability of the ensemble members (Chen & Oliver, 2016).

In simple terms, localization determines which observations can contribute to and how much they influence the update of a parameter. When dealing with permeability and porosity parameters in petroleum reservoir models, localization is commonly based on the distance between the physical locations of the parameters and observations (Chen & Oliver, 2016). In the context of modelling high-enthalpy geothermal reservoirs, using distance-based localization may be suitable for porosity parameters since the porosity distribution does not influence the simulated natural state and it is typically only the local porosity around the production wells that influences production observations. However, for the geothermal problem at hand, it appears that distance-based localization is not well suited to dealing with permeability and bottom boundary parameters. The reason is that those parameters influence the large-scale temperature and pressure distribution over the whole system since they control the natural state of the system.

We experimented with using PEST++IES without localization and with simple implementations of distance-based localization of permeability parameters. In both cases, the results were models which did not match the observations. Instead, we have looked at applying an adaptive localization procedure, which is based on the ensemble estimates of the correlations between the model parameters and observations (Luo & Bhakta, 2018). PEST++IES now, conveniently, includes an adaptive localization scheme based on the one proposed in (Luo & Bhakta, 2018). Applying PEST++IES with the adaptive localization option, we were able to obtain good matches to observations for the test cases we looked at. Therefore, the results reported here for PEST++IES were found using adaptive localization.

2.4.2 ESMDA

The ESMDA method (Emerick & Reynolds, 2013) closely resembles the Gauss-Newton variant of EnRML. Using N_a ESMDA iterations, the ensemble of models is updated at the (k+1)th iteration according to

$$\boldsymbol{m}_j^{k+1} = \boldsymbol{m}_j^k + \Delta \boldsymbol{M}_k \Delta \boldsymbol{D}_k^T [\Delta \boldsymbol{D}_k \Delta \boldsymbol{D}_k^T + \alpha_{k+1} \boldsymbol{C}_\mathrm{d}]^{-1} \left(\boldsymbol{d}_{\mathrm{obs},j}^k - \boldsymbol{d}\left(\boldsymbol{m}_j^k\right) \right) \tag{12}$$

where, at each iteration, we resample the observation realizations using $\boldsymbol{d}_{\mathrm{obs},j}^k \sim \mathcal{N}(\boldsymbol{d}_\mathrm{obs}, \alpha_{k+1}\boldsymbol{C}_\mathrm{d})$. This is unlike RML or EnRML where an ensemble member has a fixed observation realization. Here the values α_{k+1} are inflation factors for the observation noise and should satisfy

$$\sum_{k=1}^{N_a} \frac{1}{\alpha_k} = 1 \tag{13}$$

For approximately solving (12), we use the subspace inversion scheme in (Emerick, 2016; Evensen, 2009).

Standard implementations of ESMDA usually predefine the number of iterations used (see, e.g., (Emerick & Reynolds, 2013)) (though there are implementations that choose the number of iterations adaptively (Emerick, 2016)). Here we decided to use 10 ESMDA iterations and following (Emerick, 2019) we used inflation factors satisfying

$$\alpha_{k+1} = \gamma^k \alpha_1 = \gamma^{k+1-N_a} \alpha_{N_a} \tag{14}$$

where $\alpha_{N_a} = 1.5$ and $\gamma = 0.3333$.

Like with PEST++IES, we tried ESMDA along with localization. As before, we were unsuccessful when trying distance-based localization. Surprisingly, when using our ESMDA implementation, we found that using adaptive localization like the one in PEST++IES resulted in worse matches than not using localization. For ESMDA, we therefore report results found without using localization.

2.5 Computational Cost of Uncertainty Quantification Methods

Table 1 presents a simplified comparison of the computational expense associated with the uncertainty quantification methods discussed above. The overall computational expense of using RML is about N_e times higher than using the Laplace method. However, when running all RML inversions simultaneously in parallel on a computing cluster, then the time needed by the RML approach may be comparable to using the Laplace approach. Note that typically we would run simulations using the ensemble of models generated by the Laplace approach to check whether they are consistent with the observations. If the target is to generate models that satisfy (8), then the Laplace approach may require running a substantial number of additional simulations as suggested by the results presented below and in (Liu & Oliver, 2003).

As noted by White (2018), the computational cost of running an iterative ensemble smoother may be comparable to solving a single inverse problem using an industry-standard inversion method such as PEST (Doherty, 2015, 2016). For instance, if we use PEST for model updates with model sensitivities evaluated using finite differencing, the cost of a model update will be on the order of N_m simulations. However, when N_m is large, iterative ensemble smoothers typically only use $N_e \ll N_m$ simulations to update all models in the ensemble. Therefore, the computational expense of using an iterative ensemble smoother can be lower than using the Laplace approach.

For a fixed ensemble size and a fixed number of inversion iterations, the iterative ensemble smoothers are computationally less expensive than using RML, since the RML approach solves additional adjoint and direct problems. We may, therefore, be able to choose N_e larger when using the ensemble smoothers without the computational expense exceeding that of the RML approach. A larger N_e would have the benefit of reducing sampling errors and loss of ensemble variance, which is a common issue when using

iterative ensemble smoothers. However, our preliminary computational experiments suggest that for the combined natural-state and production problem the cost of a single iteration may be marginally lower for the iterative ensemble smoothers than using RML. The reason is that the computational cost is largely dominated by natural-state simulations that converge slowly, and the cost of the adjoint and direct methods is relatively low for geothermal simulations where the computational expense is dominated by natural-state simulations (Bjarkason et al., 2019; Bjarkason, 2018). For the problem presented below, the time spent on a nonlinear reservoir simulation ranged between a couple of minutes and an hour. But it consistently only took a couple of minutes to solve the adjoint and direct problems used for a single model update of an RML ensemble realization. Therefore, it is not clear which method is the most advantageous in terms of computational time. Computational cost may vary depending on the settings used for each method and the problem at hand. The primary concern is the reliability of the methods.

Table 1: A rough order of magnitude comparison of the main computational cost associated with generating an ensemble of N_e models using the methods under consideration. Here N_{IT} denotes the number of inversion iterations used by each method.

Method	Nonlinear simulations	Adjoint solves	Direct solves
Laplace	N_{IT}	$(r+l)(N_{IT}+1)$	$(r+l)(N_{IT}+1)$
RML	N_eN_{IT}	$(r+l)N_eN_{IT}$	$(r+l)N_eN_{IT}$
EnRML (PEST++IES)	N_eN_{IT}	0	0
ESMDA	N_eN_{IT}	0	0

3. EXPERIMENTAL SET-UP

For comparing the uncertainty quantification methods under consideration, we used a synthetic natural-state and production model based on the one used in (Bjarkason et al., 2018, 2016). The synthetic case is a rectangular 1.6 km by 2 km vertical slice model. The model includes the transport of heat and water, and for describing these transport processes, we use The University of Auckland's version of TOUGH2, AUTOUGH2 (Yeh et al., 2012), as the reservoir simulator. Ignoring the blocks at the top of the model, which are used to prescribe constant atmospheric boundary conditions, the model consists of 8,000 blocks. We apply the methods listed in Table 1 to estimate the log-transformed (base ten) horizontal and vertical permeabilities in each model block. This gives a total of 16,000 adjustable model parameters.

The problem we look at here differs to the one in (Bjarkason et al., 2018, 2016) in that we generate a true baseline model by sampling the true log-transformed permeability values from a Gaussian prior distribution. For details on generating the prior distribution and model truth, please refer to Chapter 7 in (Bjarkason, 2018). The true permeability values are depicted in Figure 1. The true permeability structure has anisotropic bands of low and high permeability zones. As shown in Figure 1, the true model has a low permeability cap towards the top of the model, but there is a relatively permeable pathway through the middle of the cap structure. The permeable path allows hot fluid to escape through the cap. This can be seen by looking at Figure 2, which shows block temperatures and vapour saturations at the true natural state. At natural state, there are two two-phase zones, as shown in Figure 2(b). The main two-phase zone is right above the dominant upflow zone while the secondary two-phase zone is by the top of the permeable path through the cap.

Using the true model, we generated synthetic observations in the same way as in (Bjarkason et al., 2018, 2016). Temperature measurements were taken in each of the five natural-state observation wells shown in Figure 3. Temperature measurements were taken every 60 m, giving 135 observations. For the final synthetic natural-state observations, we added Gaussian noise with zero mean and a standard deviation of 0.5°C. The natural-state temperature observations are shown in Figure 4. As production observations, we assumed a three-year production history, and took the production observations to be the production enthalpies and pressures at the bottom of the three production wells shown in Figure 3. Taking measurements every three months at all production wells gave 36 pressure observations and 36 enthalpy observations. We also added Gaussian noise to the production data, using standard deviations of 0.1 bar and 10 kJ/kg for pressures and enthalpies, respectively. The resulting production observations are shown in Figure 5. Here we look, firstly, at how well the methods listed in Table 1 can generate models that match these observations. Secondly, we consider how well the ensemble of models generated by those methods can predict production enthalpies at the three production wells during the three years that follow the historical production period.

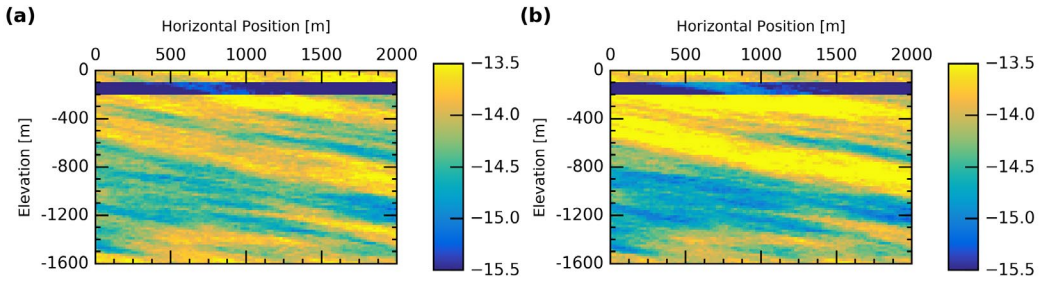

Figure 1: True log-transformed (base ten) (a) horizontal and (b) vertical permeabilities.

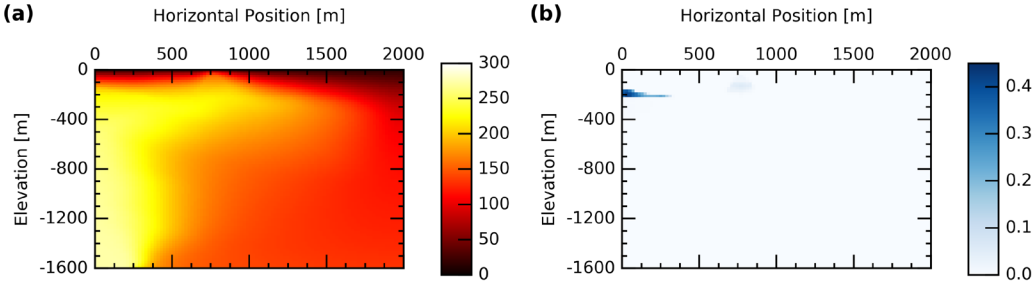

Figure 2: True natural-state (a) temperatures [°C] and (b) vapour saturations.

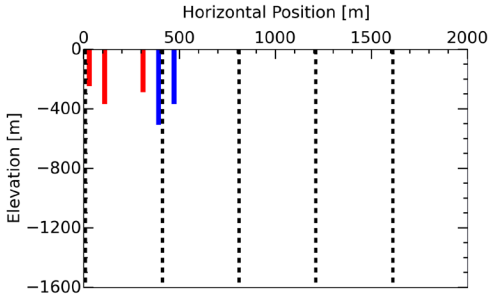

Figure 3: Location of the three production wells (red), two injection wells (blue), and five natural-state observation wells (black dashed lines).

4. RESULTS

We applied RML, PEST++IES and ESMDA to the synthetic problem described in the previous section. Initially, we ran each method using 100 ensemble members. The prior parameter ensemble was the same for all methods. The prior predicted natural-state temperatures and production observations are shown in Figures 4 and 5. As shown in Figures 4 and 5, the prior ensemble gives a wide range of predicted observations. The prior parameter mean for the log-transformed vertical permeabilities is shown in Figure 6 along with the log-transformed vertical permeabilities for the first five ensemble members of the unconditional or prior parameter ensemble. Here we will make do with comparing results for the log-transformed vertical permeabilities, and we omit showing results for the horizontal permeabilities.

As the computational efficiency of the iterative ensemble smoothers is limited by the slowest simulations, we decided to limit all forward simulations to a maximum elapsed real time of 1 hour. When a simulation exceeded that maximum time limit, we discarded the respective ensemble member. For consistency, we also terminated the inversion of the *j*th RML ensemble member when the *j*th ensemble resulted in a simulation exceeding 1 hour.

The RML and PEST++IES methods were run up to a maximum number of 15 iterations. Figure 7 compares the convergence of the RML method and the two iterative ensemble smoothers. The general converge trend of all three methods looks similar. The PEST++IES method looks like it converged at about 11 iterations. Based on this, we chose to run the ESMDA method for 10 iterations. We also tried running the ESMDA method for 15 iterations, but the final converged results looked similar to before.

Figure 8 gives more details by comparing the final values of the normalized observation mismatches (8) found by the three ensemble-based methods. The main thing to note is that RML resulted in better matches to observations than the iterative ensemble smoothers. For this type of synthetic problem, we expect that good models should give a normalized observation mismatch term which takes a value close to one (Oliver et al., 2008) (this is reflected in the bounds given in equation (8)). The RML samples are mostly consistent with this expectation, unlike the iterative ensemble smoothers which gave no posterior samples that fulfil (8) (when N_e=100).

Apart from a tendency to give suboptimal matches to observations, another concern when using iterative ensemble smoothers is that they can result in an underestimation of posterior parameter variability. This can result in an underestimation of model uncertainty and, therefore, inadequate model predictions. Figure 9 compares ensemble estimates of the posterior parameter variance of the log-transformed vertical permeabilities. The results suggest that the iterative ensemble smoothers (using N_e=100) resulted in an underestimation of parameter variability. This was especially the case for the ESMDA method. The RML approach did a better job of maintaining parameter variability and the RML posterior parameter variance looks similar to the variance estimated using the Laplace method (compare Figures 9(a) and 9(b)).

To improve the model matches and ensemble variability found using the iterative ensemble smoothers, we can use a larger ensemble size. Here we tried rerunning the ensemble smoothers using 500 ensemble members. Figure 9 demonstrates that increasing the ensemble size did indeed improve the posterior parameter variability. Likewise, Figure 8 shows that increasing the ensemble size resulted in better matches to observations when using PEST++IES. However, the improvement was marginal for the ESMDA method.

Figure 10 compares the mean of the generated posterior ensembles and selected conditional posterior samples found using the ensemble-based methods. Comparing the results in Figure 10 with the true log-transformed vertical permeabilities shown in Figure 1(b), it appears that all methods have captured the main large-scale features of the true model. These features include the permeable

path through the cap and the large bands of high and low permeability in the reservoir below the cap. What stands out the most is that the results using PEST++IES with 100 ensemble members resulted in models which look noisy or less smooth than those found using the other methods. This appears to be a result of the adaptive localization method since we got the same type of results when using ESMDA with adaptive localization. Note that this issue does not appear in the results using PEST++IES with 500 ensemble members since the larger ensemble size alleviates sampling errors.

Finally, we compared the predictive performance of the uncertainty quantification methods by looking at how well they predicted production enthalpies up to six years of production (see Figure 11). Most of the ensemble-based methods did a good job predicting the future production enthalpies in Producers 1 and 2, in the sense that the true model response is mostly contained within the intervals predicted by the ensembles. The exceptions are the predictions found using the ESMDA method with N_e=100, which gave too narrow prediction intervals because of its lack of ensemble variability.

The production enthalpies at Producer 3 were the most difficult to predict. This appears to be because Producer 3 starts producing two-phase fluid at the end of the observation period and there is only the final observation at Producer 3 that suggests the phase transition. All the methods using 100 ensemble members struggled to quantify the uncertainty in the future production enthalpies at Producer 3. However, by using a larger ensemble, the iterative ensemble smoothers did a decent job of estimating the uncertainty of the production enthalpies at all three producers. We were surprised to see that the RML method did not give better predictive intervals than it did for Producer 3. The reason for this appears to, partly, be a combination of the small ensemble size and a lack of convergence of the RML inversions. As Figure 11(f) shows, the RML ensembles tend to underpredict and give bad matches to the last observed enthalpy at Producer 3. The ensemble smoothers, on the other hand, tended to give better matches to that observation. This likely explains why they gave predictions that were generally closer to the true values for Producer 3. By running the RML inversions for additional five iterations, we found that the uncertainty quantification improved a bit for the predicted enthalpies. This is in part because individual ensembles gave better matches to the final observation enthalpy at Producer 3. Another reason is that using a larger number of iterations resulted in the number of ensembles that fulfilled (8) rising from 52 to 66. In practice, we may commonly come across this issue of incomplete convergence, which may result in inadequate uncertainty quantification.

For reference, the top row of Figure 11 shows predictions found by sampling 1,000 models from the Laplace approximation. These Laplace samples resulted in a wide range of predicted enthalpies, which contain the true model response. However, as Figure 8 shows, the Laplace sampled models gave bad matches to the observations. None of the Laplace sampled models resulted in simulated observations fulfilling (8). We noticed that the Laplace samples resulted in certain predicted natural-state observations being on average biased by up 10°C. Therefore, there could be certain predictive measures that the Laplace approach would not capture adequately. However, these preliminary results are not extensive enough to give concrete advice on which of the methods we considered should be preferred.

5. CONCLUSIONS

We looked at applying ensemble-based algorithms for uncertainty quantification of combined natural-state and production models describing high-enthalpy, geothermal reservoirs. We compared four different methods for estimating the uncertainty in future production enthalpies of a synthetic geothermal reservoir. These methods include RML, two types of iterative ensemble smoothers and the Laplace approach (local sensitivity approach). One of the main contributions of this study is that the results suggest that it may be viable to apply iterative ensemble smoothers in the context of modelling high-enthalpy reservoir models. To the best of our knowledge, the application of iterative ensemble smoothers has not been considered before in this context. It appears to be worth looking more into applying iterative ensemble smoothers in the geothermal context as they can be implemented independently of the forward model. This makes them easier to adapt to new modelling projects than using the RML approach discussed here, which applies adjoint and direct code to generate an ensemble of models that match historical observations. Furthermore, running iterative ensemble smoothers to generate an ensemble of models conditioned to observations may not necessarily require more computational time than calibrating a single model using inversion methods commonly used in the geothermal industry.

A downside of using iterative ensemble smoothers is that for practical ensemble sizes the methods tend to underestimate parameter variance and, therefore, model uncertainty. The presented results suggest that it is easier to maintain variability in the ensemble of models generated using the RML and Laplace methods. This would suggest that the Laplace and RML approaches might be less likely to underestimate model uncertainty. However, the variance reduction issue associated with iterative ensemble smoothers may be remedied to some extent by applying localization methods, but it is currently unclear what localization schemes are best suited to the geothermal context. This aspect needs further consideration when applying iterative ensemble smoothers to geothermal models.

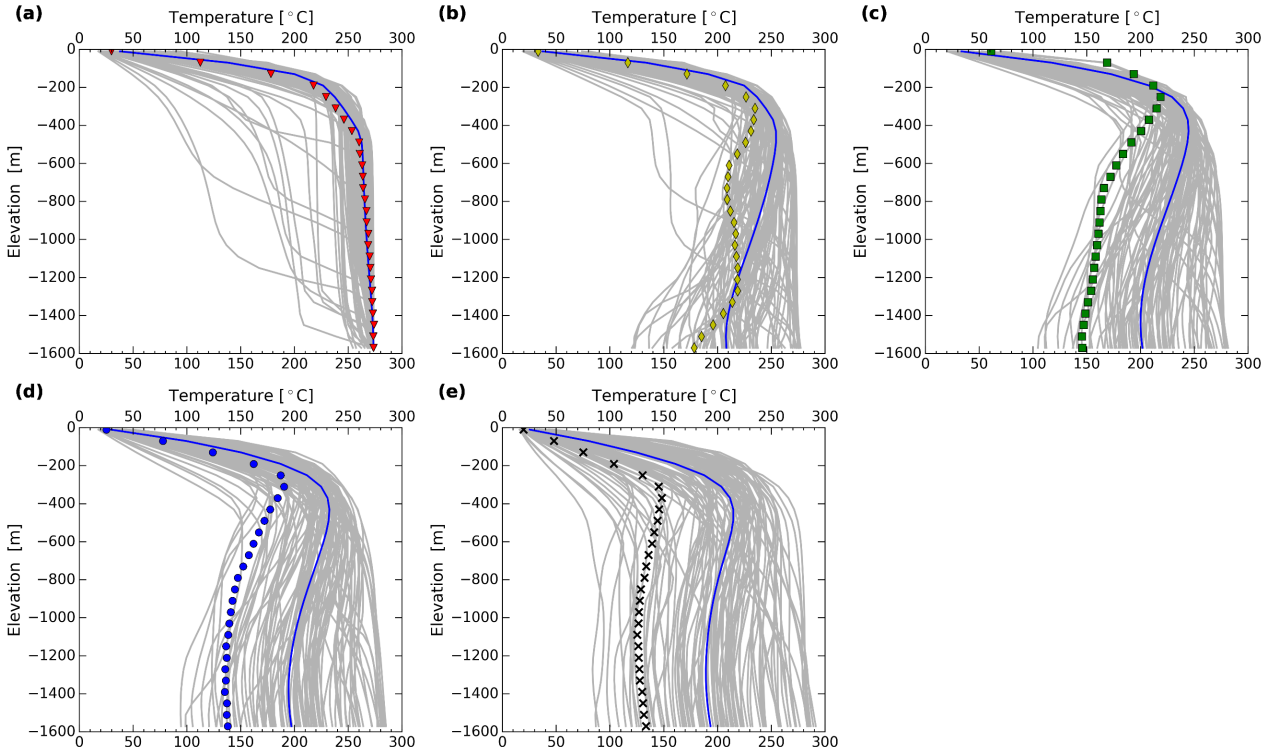

Figure 4: Natural-state temperature observations (markers), natural-state temperatures using the prior parameter mean (blue lines), and natural-state temperatures of the unconditional models (grey lines). (a) Well 1, (b) well 2, (c) well 3, (d), well 4, and (e) well 5.

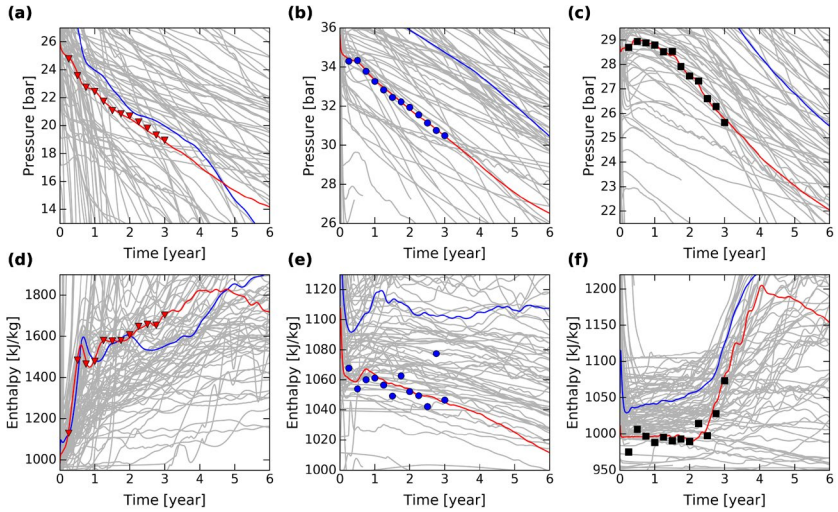

Figure 5: Predicted production pressures for (a) Producer 1, (b) Producer 2, and (c) Producer 3, when using the unconditional realizations (grey lines) and the prior mean (blue lines). Predicted production enthalpies are also shown for (d) Producer 1, (e) Producer 2, and (f) Producer 3. The markers indicate observations and the red lines show profiles using the true model.

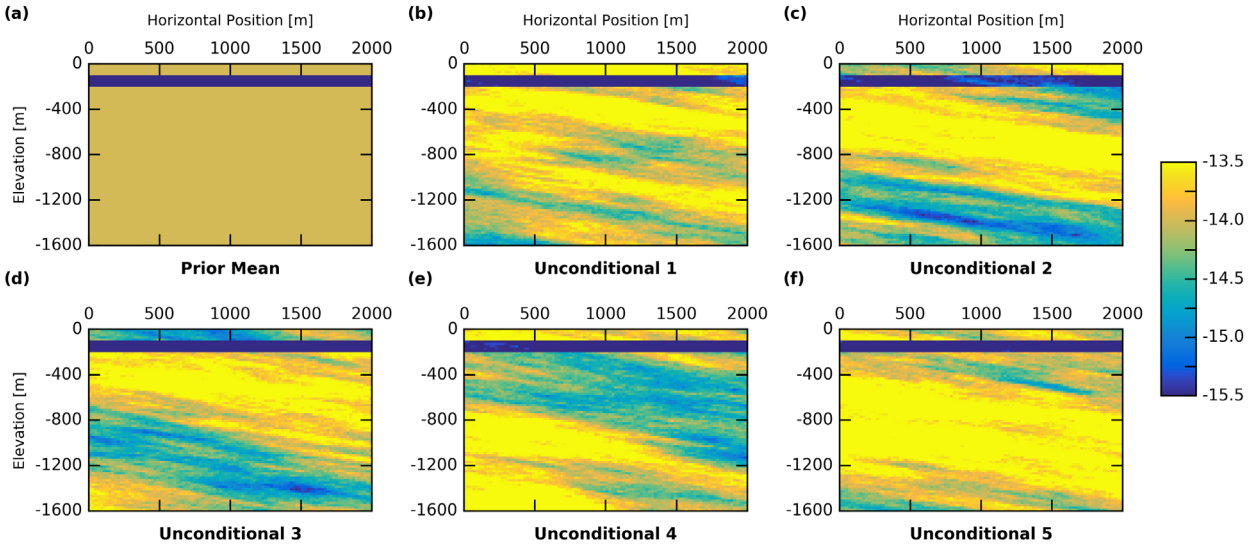

Figure 6: Log-transformed (base ten) vertical permeabilities for the (a) prior mean and (b–f) the first five unconditional (prior) ensemble members.

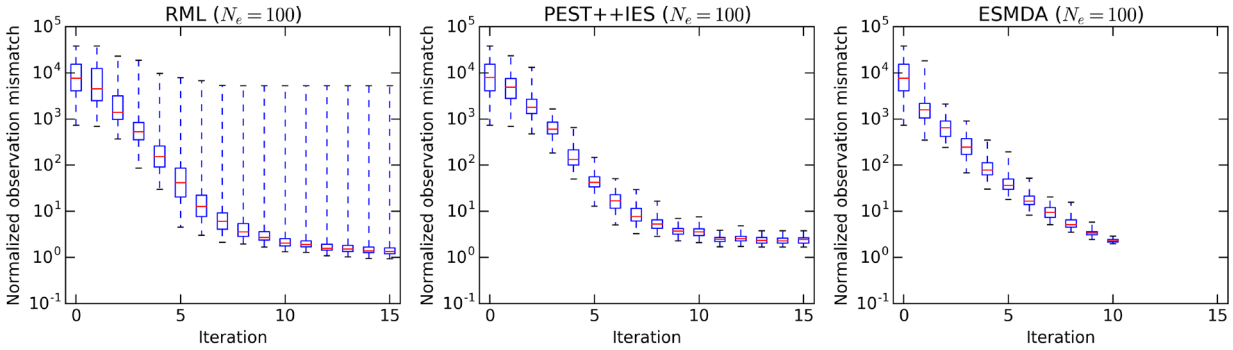

Figure 7: Boxplots showing the convergence of the RML, PEST++IES and ESMDA methods. The boxplot whiskers show the minimum and maximum values of normalized observation mismatches (8) given by the ensemble at each iteration. Red lines indicate medians, and the tops and bottoms of the blue boxes are the first and third quartiles.

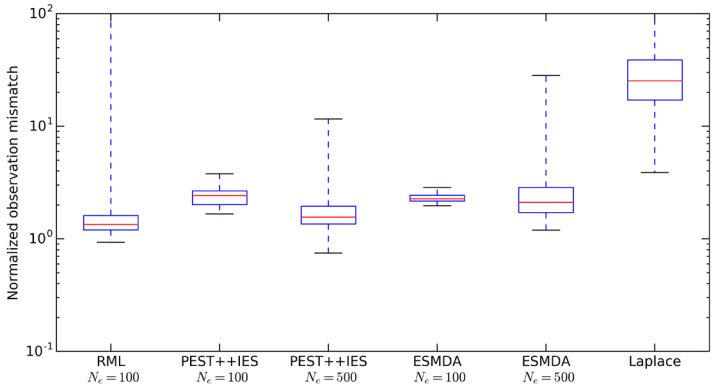

Figure 8: Boxplots of normalized observation mismatches (8) for the posterior ensembles found using the four types of uncertainty quantification algorithms considered in this study. For the two iterative ensemble smoothers (PEST++IES and ESMDA) we show results when using both 100 and 500 ensemble members. For the Laplace approximation the results are for 1,000 approximate posterior samples. The boxplot whiskers denote the minimum and maximum values, the red lines indicate medians, and the tops and bottoms of the blue boxes are the first and third quartiles.

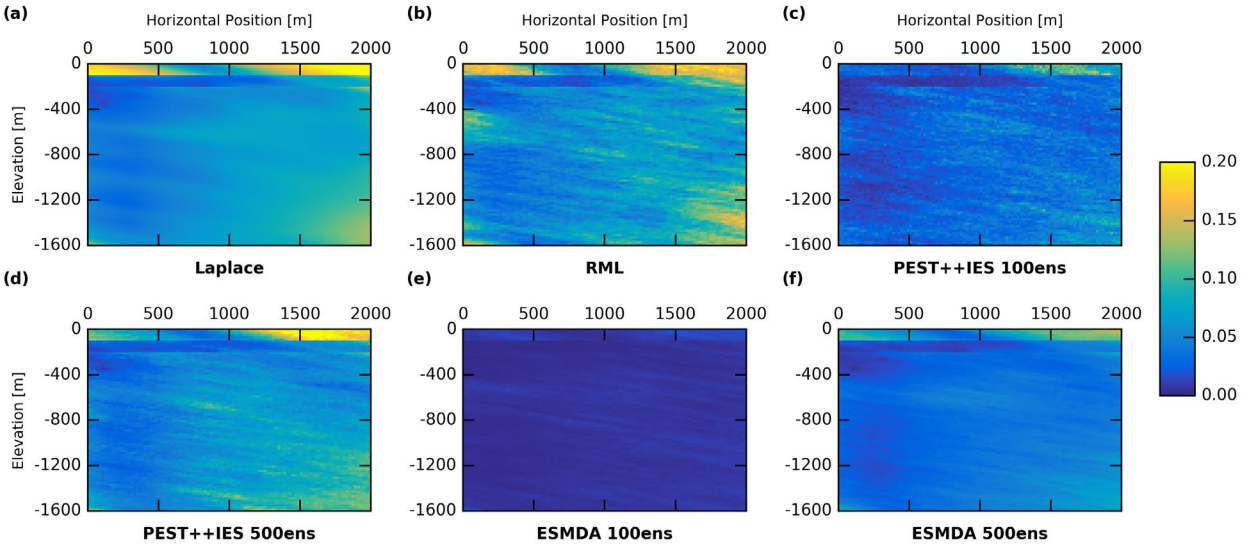

Figure 9: Estimated posterior parameter variance for the log-transformed vertical permeabilities.

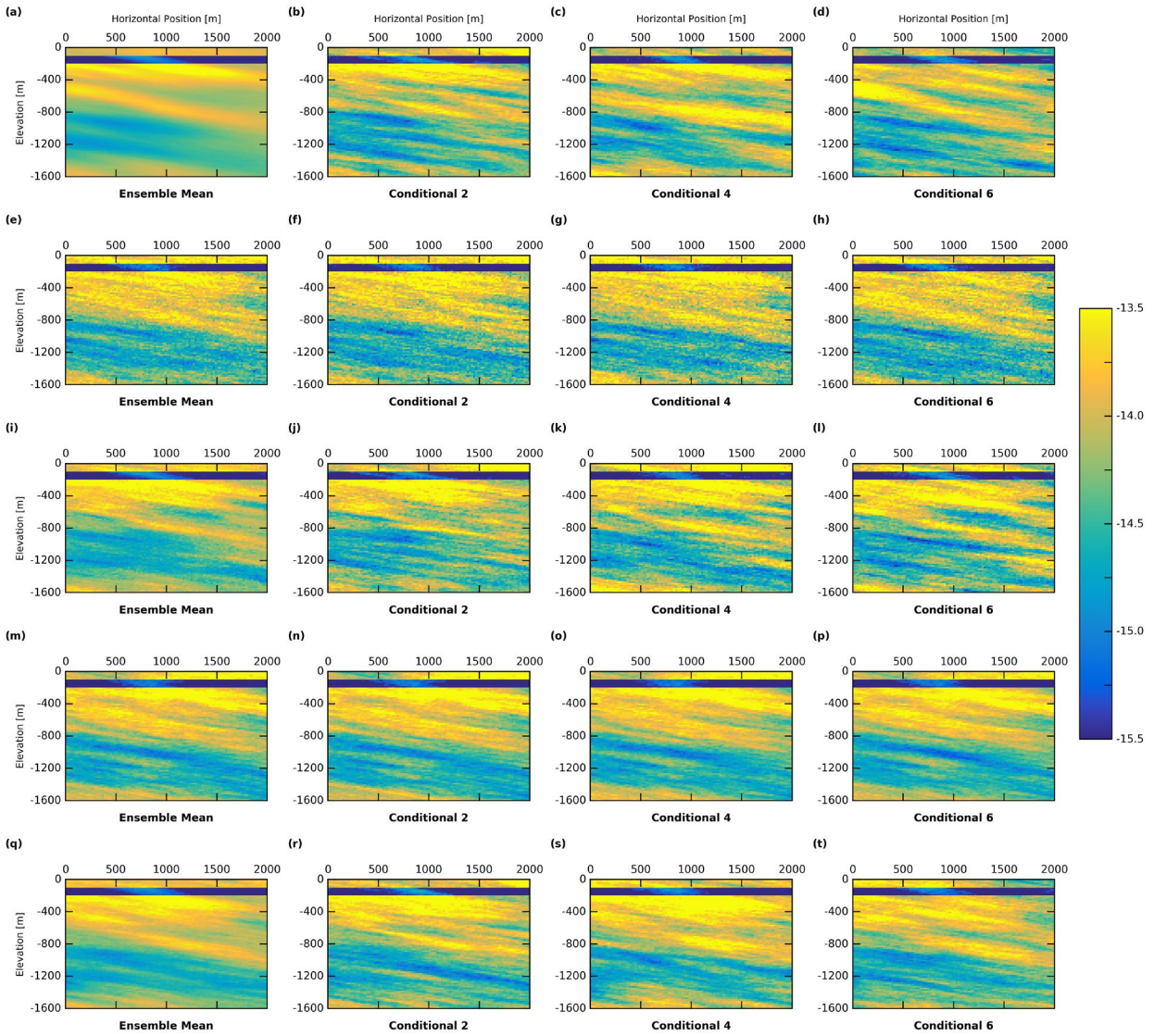

Figure 10: Posterior ensemble means for the log-transformed vertical permeabilities and the log-transformed vertical permeabilities for selected conditional ensemble members. First row: RML, second row: PEST++IES with 100 ensemble members, third row: PEST++IES with 500 ensemble members, fourth row: ESMDA with 100 ensemble members, and fifth row: ESMDA with 500 ensemble members.

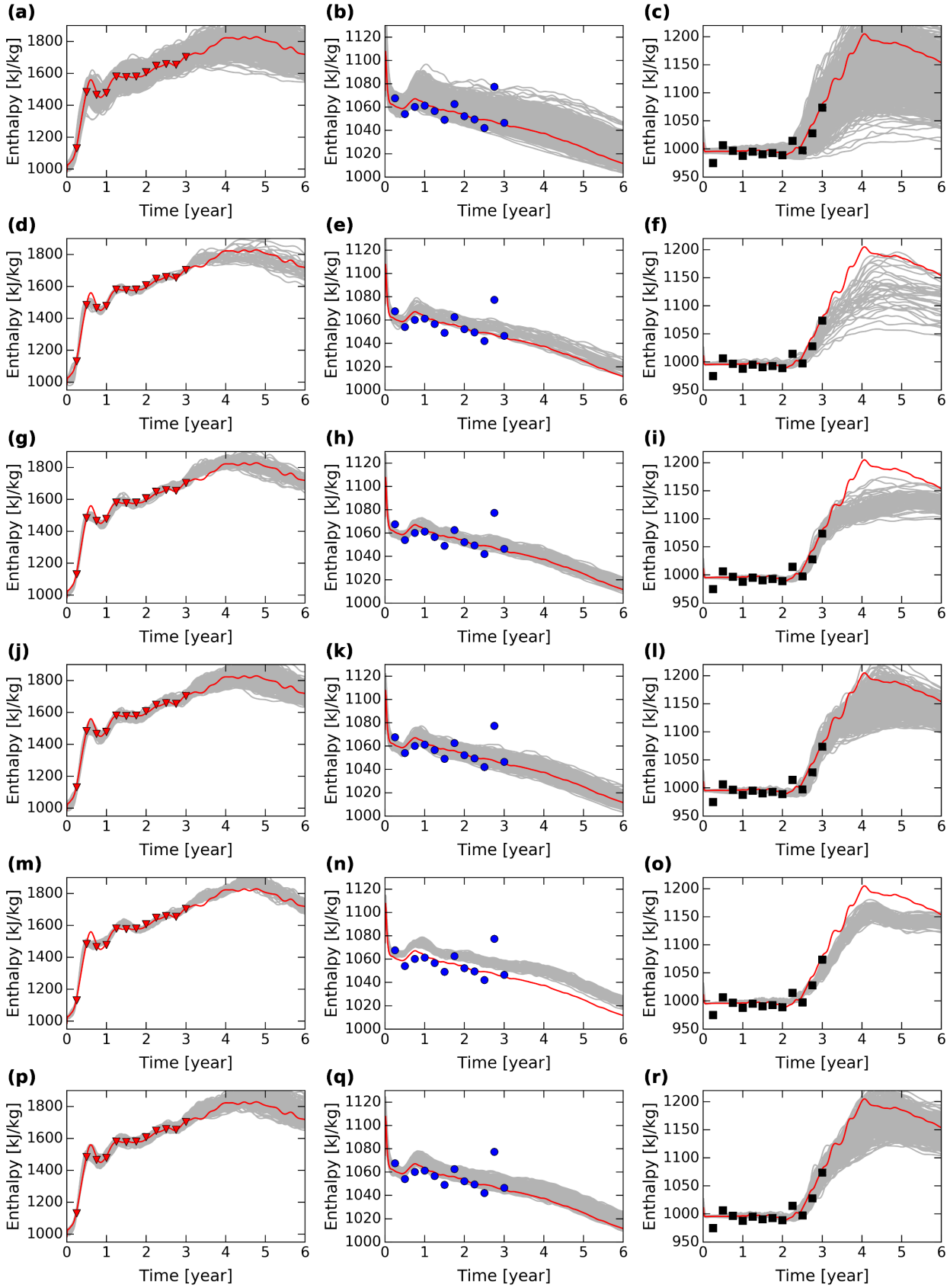

Figure 11: Ensemble enthalpy predictions using the Laplace method (top row), RML (second row), PEST++IES with N_e=100 (third row), PEST++IES with N_e=500 (fourth row), ESMDA with N_e=100 (fifth row), and ESMDA with N_e=500 (bottom row). Predicted production enthalpies are shown for Producer 1 (left column), Producer 2 (central column), and Producer 3 (right column). Gray lines denote predictions using conditional ensemble realizations, the markers indicate observations, and the red lines show predictions using the true model.

ACKNOWLEDGEMENTS

We are grateful to Landsvirkjun (the National Power Company of Iceland) for financial support provided by Orkurannsóknasjóður grant NÝR-06 - 2019. We also thank Jeremy T. White for his advice on using PEST++IES. The computational experiments were carried out using New Zealand eScience Infrastructure (NeSI) high performance computing facilities. New Zealand's national facilities are provided by NeSI and funded jointly by NeSI's collaborator institutions and through the Ministry of Business, Innovation & Employment's Research Infrastructure programme (https://www.nesi.org.nz).

REFERENCES

Bjarkason, E. K. (2018) Inversion of Geothermal Reservoir Models Using the Adjoint Method and Randomized Low-Rank Matrix Approximation Algorithms. *PhD thesis*. The University of Auckland, Auckland, New Zealand.

Bjarkason, E. K. (2019) Pass-efficient randomized algorithms for low-rank matrix approximation using any number of views. *SIAM Journal on Scientific Computing*, 41(4), A2355–A2383.

Bjarkason, E. K., Maclaren, O. J., O'Sullivan, J. P., & O'Sullivan, M. J. (2018) Randomized truncated SVD Levenberg-Marquardt approach to geothermal natural state and history matching. *Water Resources Research*, 54, 2376–2404.

Bjarkason, E. K., O'Sullivan, M. J., & O'Sullivan, J. (2014) Efficient sensitivity computations for automatic geothermal model calibration. *Proceedings 36th New Zealand Geothermal Workshop*. Auckland, New Zealand.

Bjarkason, E. K., O'Sullivan, M. J., & O'Sullivan, J. (2015) Improved sensitivity calculations. *Proceedings 37th New Zealand Geothermal Workshop*. Auckland, New Zealand.

Bjarkason, E. K., O'Sullivan, J. P., Yeh, A., & O'Sullivan, M. J. (2016) Combined natural state and history matching using the adjoint or direct sensitivity method. *Proceedings 38th New Zealand Geothermal Workshop*. Auckland, New Zealand.

Bjarkason, E. K., O'Sullivan, J. P., Yeh, A., & O'Sullivan, M. J. (2019) Inverse modeling of the natural state of geothermal reservoirs using adjoint and direct methods. *Geothermics*, 78, 85–100.

Chen, Y., & Oliver, D. S. (2013) Levenberg–Marquardt forms of the iterative ensemble smoother for efficient history matching and uncertainty quantification. *Computational Geosciences*, 17(4), 689–703.

Chen, Y., & Oliver, D. S. (2014) History matching of the Norne full-field model with an iterative ensemble smoother. *SPE Reservoir Evaluation & Engineering*, 17(2), 244–256.

Chen, Y., & Oliver, D. S. (2016) Localization and regularization for iterative ensemble smoothers. *Computational Geosciences*, 21(1), 13–30.

Doherty, J. (2015) Calibration and Uncertainty Analysis for Complex Environmental Models. PEST: Complete Theory and What it Means for Modelling the Real World. *Watermark Numerical Computing*. Brisbane, Australia.

Doherty, J. (2016) PEST: Model-Independent Parameter Estimation User Manual Part I: PEST, SENSAN, and Global Optimisers. 6th edition. *Watermark Numerical Computing*. Brisbane, Australia.

Doherty, J., Yeh, A., Colina, R., Omagbon, J. B., O'Sullivan, J. P., & O'Sullivan, M. J (2017) Experiments with inverse modelling and uncertainty quantification with a geothermal model. *Proceedings 39th New Zealand Geothermal Workshop*. Rotorua, New Zealand.

Emerick, A. A. (2016) Analysis of the performance of ensemble-based assimilation of production and seismic data. *Journal of Petroleum Science and Engineering*, 139, 219–239.

Emerick, A. A. (2019) Analysis of geometric selection of the data-error covariance inflation for ES-MDA. *Journal of Petroleum Science and Engineering*, 182, 106168.

Emerick, A. A. & Reynolds, A. C. (2013) Ensemble smoother with multiple data assimilation. *Computers & Geosciences*, 55, 3–15.

Evensen, G. (1994) Sequential data assimilation with a nonlinear quasi-geostrophic model using Monte Carlo methods to forecast error statistics. *Journal of Geophysical Research*, 99(C5), 10143–10162.

Evensen, G. (2009) Data Assimilation: the Ensemble Kalman Filter. 2nd edition. *Springer*. Berlin.

Finsterle, S. (2007) iTOUGH2 User's Guide, Report LBNL-40040. *Lawrence Berkeley National Laboratory*. Berkeley, California.

Finsterle, S., & Pruess, K. (1995) ITOUGH2: Solving TOUGH inverse problems. *Proceedings TOUGH Workshop*, 287–292. Lawrence Berkeley National Laboratory, Berkeley, California.

Halko, N., Martinsson, P. G., & Tropp, J. A. (2011) Finding structure with randomness: Probabilistic algorithms for constructing approximate matrix decompositions. *SIAM Review*, 53, 217–288.

Houtekamer, P. L., & Mitchell, H. L. (2005) Ensemble Kalman filtering. *Quarterly Journal of the Royal Meteorological Society*, 131(613), 3269–3289.

Liu, N., & Oliver, D. S. (2003) Evaluation of Monte Carlo methods for assessing uncertainty. *SPE Journal*, 8(2), 188–195.

Luo, X., & Bhakta, T. (2018) Towards automatic and adaptive localization for ensemble-based history matching. *Proceedings 16th European Conference on the Mathematics of Oil Recovery, ECMOR XVI.*

Miyoshi, T., Lien, G.-Y., Satoh, S., Ushio, T., Bessho, K., Tomita, H., et al. (2016) "Big Data Assimilation" Toward post-petascale severe weather prediction: An overview and progress. *Proceedings of the IEEE*, 104(11), 2155–2179.

Oliver, D. S., He, N., & Reynolds, A. C. (1996) Conditioning permeability fields to pressure data. *Proceedings European Conference on the Mathematics of Oil Recovery V*. Leoben, Austria.

Oliver, D. S., Reynolds, A. C., & Liu., N. (2008) Inverse theory for petroleum reservoir characterization and history matching. 1st edition. *Cambridge University Press*.

Omagbon, J. B. (2018) Linear analysis as a practical method for quantifying the uncertainty of geothermal models. *PhD thesis*. The University of Auckland, Auckland, New Zealand.

Onur, M., & Tureyen, O. I. (2006). Assessing uncertainty in future pressure changes predicted by lumped-parameter models for low temperature geothermal systems. *Proceedings 31st Workshop on Geothermal Reservoir Engineering*. Stanford University, Stanford, California.

Petra, N., Martin, J., Stadler, G., & Ghattas, O. (2014) A computational framework for infinite-dimensional Bayesian inverse problems, part II: Stochastic Newton MCMC with application to ice sheet flow inverse problems. *SIAM Journal on Scientific Computing*, 36(4), A1525–A1555.

Tureyen, O. I., Kırmacı, A., & Onur, M. (2014) Assessment of uncertainty in future performance predictions by lumped-parameter models for single-phase liquid geothermal systems. *Geothermics*, *51*, 300–311.

Tureyen, O. I., & Onur, M. (2010) Assessing uncertainty in future performance predictions of lumped parameter models using the randomized maximum likelihood method. *Proceedings World Geothermal Congress 2010*. Bali, Indonesia.

Tureyen, O. I., & Onur, M. (2011) Investigation of the use of the ensemble Kalman filter (EnKF) for history matching pressure data from geothermal reservoirs. *Proceedings 36th Workshop on Geothermal Reservoir Engineering*. Stanford University, Stanford, California.

Vogt, C., Marquart, G., Kosack, C., Wolf, A., & Clauser, C. (2012) Estimating the permeability distribution and its uncertainty at the EGS demonstration reservoir Soultz-sous-Forêts using the ensemble Kalman filter. *Water Resources Research*, 48(8).

Welter, D. E., White, J. T., Doherty, J. E., & Hunt, R. J. (2015) PEST++ version 3, a parameter estimation and uncertainty analysis software suite optimized for large environmental models. In: *U.S. Geological Survey Techniques and Methods Report*.

White, J. T. (2018) A model-independent iterative ensemble smoother for efficient history-matching and uncertainty quantification in very high dimensions. *Environmental Modelling & Software*, 109, 191–201.

Yeh A., Croucher A. E, & O'Sullivan M. J. (2012) Recent developments in the AUTOUGH2 simulator. *Proceedings TOUGH Symposium*. Lawrence Berkeley National Laboratory, Berkeley, California.

Zhang, Z., Jafarpour, B., & Li, L. (2014) Inference of permeability heterogeneity from joint inversion of transient flow and temperature data. *Water Resources Research*, 50, 4710–4725.